Journal of Functional Foods 135 (2025) 107104

Contents lists available at ScienceDirect

Journal of Functional Foods

journal homepage: www.elsevier.com/locate/jff

Rhubarb polysaccharides alleviate hypertriglyceridemia-induced acute pancreatitis and regulate gut microbiota-mediated tryptophan metabolism

Ya Chen [a,1], Wen-Wen Zhang [b,1], Yun-Yun Mao [a], Gang-Ao Hu [b], Xin-Xin Chen [a], Yi-Lin Zhou [b], Xiao-Long Chen [a], Hong Wang [b,*], Bin Wei [b,*], Jian-Feng Tu [a,c,**]

[a] Emergency and Critical Care Center, Department of Emergency Medicine, Zhejiang Provincial People's Hospital, Affiliated People's Hospital, Hangzhou Medical College, Hangzhou 310014, Zhejiang, PR China
[b] College of Pharmaceutical Science & Collaborative Innovation Center of Yangtze River Delta Region Green Pharmaceuticals, Zhejiang key laboratory of green, low-carbon, and efficient development of Marine Fishery Resources, Zhejiang University of Technology, Hangzhou 310014, China.
[c] Second Clinical Medical College Hangzhou Normal University Hangzhou, Hangzhou 310014, Zhejiang, PR China

ARTICLE INFO

Keywords:
Rhubarb polysaccharides
Hypertriglyceridemia-induced pancreatitis
Gut microbiota
Metabolomics
Tryptophan metabolism

ABSTRACT

Rheum tanguticum plays a key role in treating acute pancreatitis, though its bioactive components and mechanisms remain unclear. This study investigates the structural characteristics and therapeutic effects of rhubarb polysaccharides (RP) in a mouse model of hypertriglyceridemia-induced acute pancreatitis (HTGAP). The isolated polysaccharide, (26 kDa, primarily glucose and arabinose) significantly reduced serum amylase and lipase levels, improved pancreatic and intestinal histopathology and upregulated tight junction proteins Zonula Occludens-1 and Occludin. High throughput 16S rRNA sequencing demonstrated that RP supplementation modulated gut microbiota by enriching beneficial genera (e.g., *Lactobacillus* and *Akkermansia*) while reducing pathogenic genera (*Lachnoclostridium*, *Desulfovibrio*). Untargeted metabolomics revealed alterations in microbial metabolites, particularly in the tryptophan metabolism. Integrated analysis revealed significant microbiota-metabolite correlations. These findings suggest that RP improve HTGAP by restoring intestinal barrier integrity and regulating gut microbiota-mediated tryptophan metabolism, highlighting its potential as a therapeutic agent.

1. Introduction

Hypertriglyceridemia-induced acute pancreatitis (HTGAP) is the third leading cause of acute pancreatitis after gallstones and alcohol, with its incidence increasing annually (Yao et al., 2024). It is clinically characterized by younger onset, higher rates of severe cases, frequent recurrence, and multiple complications (de Pretis et al., 2018; Yao et al., 2024). The pathogenesis of HTGAP is closely associated with lipid metabolism disorders, systemic inflammatory responses, and multi-organ dysfunction (Song et al., 2023). Although triglyceride (TG)-lowering therapies (e.g., fasting, oral medications, insulin, heparin, and blood purification) have been widely adopted for HTGAP management (Gubensek, 2023), recent clinical evidence has questioned their efficacy. Clinical studies indicate that therapeutic interventions including intravenous heparin administration, insulin infusion (with concurrent glucose infusion to prevent hypoglycemia in normoglycemic patients) and plasma exchange exhibit no significant efficacy in managing HTGAP. Consequently, current guidelines advise against the routine use of triglyceride-lowering therapies for HTGAP treatment (Syed-Abdul et al., 2025). However, pharmacological interventions are often accompanied by adverse effects. Given the limitations of conventional therapies, there is an urgent need to explore alternative treatment strategies with better safety profiles and novel mechanisms of action.

In this context, traditional Chinese medicine (TCM) has emerged as a promising therapeutic agent for various diseases. Furthermore, medicinal plants have been shown to be effective against parasitic foodborne illnesses (Iqbal et al., 2024), demonstrating the potential to modulate gut microbiota and metabolic processes. Gut microbiota is a complex community of microorganisms residing in the human intestinal tract. Collectively, they form a biological barrier within the intestinal mucosa

* Corresponding authors at: 18 Chaowang Road, Xiacheng District, Hangzhou, Zhejiang Province, PR China.
** Corresponding author at: 158 Shangtang Road, Hangzhou, Zhejiang Province, PR China.
E-mail addresses: hongw@zjut.edu.cn (H. Wang), binwei@zjut.edu.cn (B. Wei), zjpph-ap@hmc.edu.cn (J.-F. Tu).
[1] Ya Chen and Wen-Wen Zhang contributed equally to this work.

https://doi.org/10.1016/j.jff.2025.107104
Received 15 October 2025; Received in revised form 15 November 2025; Accepted 16 November 2025
Available online 19 November 2025

(Du et al., 2025; Yi et al., 2025). Beyond its roles in energy metabolism, host defense, and immune regulation, the gut microbiota is closely linked to various diseases such as diabetes mellitus (Wu et al., 2020), obesity (Wu et al., 2024), and pancreatitis (Liu et al., 2024). Notably, it plays a critical role in the pathogenesis and progression of HTGAP. Studies have revealed that HTGAP patients exhibit gut dysbiosis (e.g., an elevated Firmicutes/Bacteroidetes ratio) (Hu et al., 2021), leading to degradation of the intestinal mucus layer and downregulation of tight junction proteins Zonula Occludens-1 (ZO-1) and Occludin. Furthermore, the gut microbiota can metabolically transform active components of TCM through biotransformation processes such as catabolism or structural modification, thereby altering their bioavailability and therapeutic efficacy (Gou et al., 2023). The intricate relationship between TCM and gut microbiota suggests that targeting this axis may represent a novel therapeutic approach for HTGAP management.

Building upon this concept, polysaccharides are bioactive extracts with diverse pharmacological properties, including hepatoprotective, hypoglycemic, antioxidant, anti-inflammatory, antitumor, and immunomodulatory effects. Rhubarb, a traditional Chinese medicinal herb widely used in treating gastrointestinal disorders, contains primary bioactive constituents such as anthraquinones, anthrones, stilbenes, tannins, and polysaccharides (Cao et al., 2017; Xu et al., 2021). Rhubarb polysaccharides (RP) have been shown to ameliorate non-alcoholic fatty liver disease (NAFLD) by inhibiting lipid accumulation and reducing inflammatory damage in hepatocytes (Qiu et al., 2025). Additionally, RP modulates gut microbiota and suppresses pro-inflammatory cytokine secretion in murine colitis models via regulation of the Notch and Nuclear Factor-κB (NF-κB) signaling pathways (Zhang et al., 2023). However, current research predominantly focuses on the therapeutic efficacy of emodin, an anthraquinone derivative from rhubarb, in acute pancreatitis (Wen et al., 2020; Yang, Han, et al., 2023). Notably, there remain a significant lack of research on the therapeutic efficacy of RP in HTGAP, particularly their definitive anti-inflammatory effects and primary mechanisms mediated by gut microbiota.

Therefore, the present study aimed to: (1) isolate and structurally characterize the polysaccharide from *Rheum tanguticum*; (2) evaluate its therapeutic efficacy against HTGAP in a murine model; and (3) elucidate the underlying mechanisms, with a specific focus on its interplay with the gut microbiota and host metabolism, using integrated 16S rRNA gene sequencing and untargeted metabolomics approaches.

2. Materials and methods

2.1. Extraction of rhubarb polysaccharides

Rheum tanguticum was purchased from Zhejiang Chinese Medical University Chinese Herbal Pieces Co., Ltd. (Place of Origin: Gansu, Batch Number: 240101) in April 2023. The experimental procedure was adapted from a previous study (Zhang et al., 2023). Approximately 50 g of *Rheum tanguticum* roots were soaked overnight in 95 % ethanol to remove liposoluble components and partial pigments. The filtered residue was air-dried, then decocted with 10 volumes of water (*v/w*) for 1 h. After filtration, the marc was subjected to two additional decoctions with 10 volumes of water each. The three extracts were combined, concentrated to 2 L under reduced pressure, and mixed with four volumes of 95 % ethanol under stirring, followed by overnight standing. The brown-black precipitate was collected by centrifugation, sequentially washed with anhydrous ethanol and diethyl ether, and vacuum-dried to obtain RP (~4 g).

2.2. Structure characterization of rhubarb polysaccharides

The Fourier transform infrared (FTIR) spectrometer (BRUKER TENSOR 27, Germany) was employed to analyze the infrared spectra of the polysaccharide samples. A small amount of the RP sample was mixed with 200 mg of potassium bromide (KBr), compressed into a pellet, and scanned over the wavenumber range of 400–4000 cm^{-1}. Structural features were interpreted based on characteristic absorption peaks. For monosaccharide composition analysis, liquid chromatography-mass spectrometry (LC-MS) was utilized with minor modifications (Yu et al., 2025). The RP sample (1.5 mg) was hydrolyzed with 1 mL of trifluoroacetic acid (TFA, 4 mol/L) at 110 °C for 4 h. Subsequently, 200 μL of methanol was added, and the sample was dried via nitrogen blowing 2–3 times. The residue was then derivatized with 0.5 M 1-phenyl-3-methyl-5-pyrazolone (PMP) in a 70 °C water bath for 30 min. The solution was neutralized using HCl, followed by chloroform extraction. The supernatant was filtered through a 0.22 μm membrane and analyzed and their relative contents were quantified using chromatographic peak areas. Size exclusion chromatography (SEC) was applied to assess the molecular weight distribution and homogeneity of *Rheum palmatum* polysaccharide components. Additionally, Ultraviolet-Visible Spectrophotometry (UV–Vis) absorption spectroscopy was performed on the polysaccharide samples, and characteristic absorption peaks were recorded.

2.3. Animal experiment

Six- to seven-week-old male C57BL/6 mice (18–20 g) at specific pathogen-free (SPF) grade were purchased from Hangzhou Qizhen Laboratory Animal Technology Co., Ltd. The mice were housed in a ventilated cage system under controlled conditions: temperature (25.0 ± 0.5) °C, humidity (55 ± 5) %, and a natural light/dark cycle. Mice were randomly divided into 3 groups ($n = 6$/group): (1) Normal control (NC) group, (2) HTGAP group, and (3) RP group. The method we used to establish the HTGAP model was primarily adapted from (Yang et al., 2022; Yang, Luo, et al., 2023), with minor modifications. To induce HTGAP, after 1-week acclimatization, mice received intraperitoneal injections of P-407 (poloxamer 407, MCE) every other day for 7 days (0.5 g/kg). Subsequently, L-Arg (L-arginine, Sigma-Aldrich) was injected twice at 1 h intervals (2.5 g/kg). Controls received saline. One hour after the second injection of L-Arg, 200 mg/kg of RP was administered orally, followed by two additional doses at 6-h intervals. All mice were fasted for 12 h before modeling. At 24 h after the first L-Arg injection, blood was collected via orbital puncture, and mice were euthanized by cervical dislocation. Pancreatic/colonic tissues and cecal contents were harvested for analysis. All procedures were approved by Zhejiang University of Technology (Approval No. ZH20240716021) and complied with institutional guidelines.

2.4. Serum amylase and lipase determination

Blood samples were collected in 1.5 mL sterile Eppendorf tubes and allowed to clot at room temperature for 2 h prior to centrifugation. The serum was separated by centrifugation at 3000 rpm for 15 min at 4 °C. Amylase (Kit No. C016–1) and lipase (Kit No. A054–2) activities were measured using commercial kits (Nanjing Jiancheng Bioengineering Institute, China) following the manufacturer's instructions. Absorbance was recorded with an ELx800™ Microplate Reader (BioTek, USA).

2.5. Histological assessment

Pancreatic and colonic tissues were fixed in 4 % (*w/v*) paraformaldehyde, dehydrated, embedded in paraffin, and sectioned at 5 μm thickness for hematoxylin and eosin (HE) staining. Pancreatic histopathology was scored under a light microscope according to established criteria (Pan et al., 2017). Colonic morphology was scored under a light microscope (Shen et al., 2024).

2.6. Immunohistochemistry staining

The expression of intestinal barrier proteins ZO-1 and Occludin was evaluated in paraffin-embedded colon tissues by

immunohistochemistry. In brief, tissue sections were deparaffinized and rehydrated, followed by heat-induced antigen retrieval in citrate buffer (pH 6.0) at 95 °C for 15–20 min. Endogenous peroxidase activity was quenched by treating the sections with 3 % hydrogen peroxide for 10 min. The sections were then incubated at room temperature for 1 h with the following rabbit primary antibodies: anti–ZO-1 (Huaan, Cat# HA722797, dilution 1:100) and anti–Occludin (Huaan, Cat# ET1701–76, dilution 1:200). After washing, the corresponding horseradish peroxidase (HRP)-conjugated secondary antibody was applied. Immunoreactivity was visualized using a 3,3′-diaminobenzidine (DAB) substrate, and nuclei were counterstained with hematoxylin. All stained sections were examined under a Nikon optical microscope at 200× magnification. Quantitative analysis of protein expression, represented as integrated optical density per unit area (AOD), was performed using Image-Pro Plus 6.0 software (Media Cybernetics Inc., Bethesda, MD, USA).

2.7. Real-time quantitative PCR

Total RNA was isolated from colonic tissues using TRIzol reagent (Vazyme Biotech Co., Ltd., China) according to the manufacturer's instructions. RNA concentration was measured with a NanoDrop™ spectrophotometer (Thermo Fisher Scientific, USA). The RNA was reverse transcribed to cDNA using a HiScript IV All-in-one Ultra RT SuperMix (Vazyme, Nanjing, China, Cat no. R433–01). Quantitative real-time PCR (RT-qPCR) was performed with ChamQ Universal SYBR qPCR Master Mix (Vazyme, Cat. No. Q711–02) on an Applied Biosystems 7500 system. Gene-specific primers (Table 1) were used, with GAPDH as the reference gene. Relative gene expression was calculated by the $2-\Delta\Delta C_t$ method.

2.8. Gut microbiota analysis by 16S rRNA gene sequencing

At the end of the experiment, cecal contents were aseptically collected, flash-frozen in liquid nitrogen, and stored at −80 °C. Microbial genomic DNA was extracted using the TGuide S96 Magnetic Soil/Stool DNA Kit (DP812, Tiangen, China). The V3-V4 region of the bacterial 16S rRNA gene was amplified with primers 338F (5'-ACTCCTACGGGAGGCAGCA-3′) and 806R (5'-GGACTACHVGGGTWTCTAAT-3′). Amplicons were sequenced on the Illumina NovaSeq 6000 platform (Tsingke Biotechnology Co., Ltd., China). Raw sequences were analyzed with QIIME2 (version 2024.2), and the OmicStudio cloud platform (https://www.omicstudio.cn/tool) was used for bioinformatics analysis, including Principal Component Analysis (PCA) to evaluate microbial community differences among groups.

2.9. Untargeted metabolomics analysis of cecal contents

Cecal contents (50 mg) were homogenized in 400 μL of methanol: water (4,1, *v*/v) using a Wonbio-96C High-throughput tissue grinder (50 Hz, 6 min, −10 °C). The mixture was vortexed for 30s, sonicated at 5 °C (40 kHz) for 30 min, and incubated at −20 °C for 30 min to precipitate proteins. After centrifugation (13,000 ×*g*, 15 min, 4 °C), the supernatant was transferred to LC-MS vials. Analysis was performed on a Thermo UHPLC-Exploris 240 mass spectrometer with an Electrospray Ionization (ESI) source (positive/negative modes). Parameters: Aux gas heater: 350 °C; Capillary temperature: 320 °C; Sheath/Aux gas flow: 60/20 psi; Ion-spray voltage: −3000 *V* (negative), 3400 V (positive); Normalized collision energy: 20–40–60 eV; MS resolution: 60,000 (full MS), 15,000 (MS/MS); Mass range: 70–1050 *m/z*. Data were acquired in Data-Dependent Acquisition (DDA) mode, processed with Progenesis QI (Waters Corporation, USA), and metabolites were identified via Human Metabolome Database (HMDB) (http://www.hmdb.ca/), Metlin (https://metlin.scripps.edu/), and the Majorbio Database. Statistical analysis was conducted on the Majorbio Cloud Platform (www.cloud.majorbio.com).

Table 1
Primes used in this study.

Gene name	Forward (5′-3′)	Reverse (5′-3′)
ZO-1	GTTGGTACGGTGCCCTGAAAGA	GCTGACAGGTAGGACAGACGAT
Occuldin	TGGCAAGCGATCATACCCAGAG	CTGCCTGAAGTCATCCACACTC
GAPDH	AATGTGTCCGTCGTGGATCTGA	GATGCCTGCTTCACCACCTTCT

2.10. Statistical analysis

Data are expressed as the mean ± standard error of the mean (SEM) values. Spearman correlation coefficients were calculated using the OmicStudio tools to construct the microbe-metabolite interaction and molecular networks (Lyu et al., 2023). For multiple comparisons, significant differences ($p < 0.05$) were performed using one-way ANOVA followed by Tukey's multiple comparisons test using version GraphPad Prism 10.0.

3. Results

3.1. Structure characteristics of RP

The structural characteristics of RP were characterized using FT-IR, LC-MS, SEC, and UV–Vis spectroscopy. As shown in Fig. 1A, the FT-IR spectrum exhibited characteristic polysaccharide absorption bands, including those of O—H, C—H, C═O, and C—N stretching vibrations. The broad absorption band between 3600 and 3200 cm^{-1} corresponds to O—H stretching vibrations, a hallmark feature of carbohydrates. A prominent peak at 3321.01 cm^{-1} further confirms the O—H stretching vibration, consistent with the saccharide structures. Based on the previously established multiple reaction monitoring method in LC-MS, the monosaccharide composition of RP was determined. RP is primarily composed of glucose, and arabinose, followed by galacturonic acid, galactose, mannose and glucuronic acid, with a molar ratio of 36:24:6:6:3:1, respectively (Fig. 1B). Gel permeation chromatography (GPC) revealed a narrow peak (retention time: 14.108 min), indicating that RP is a relatively homogeneous polysaccharide with an average molecular weight of 26 kDa (Fig. 1C). UV–Vis spectroscopy demonstrated a smooth curve between 280 and 500 nm, with no distinct absorption peaks observed at 260–280 nm, confirming the absence of nucleic acids or proteins in the RP extract (Fig. 1D).

3.2. RP supplementation alleviated pathological symptoms in HGTAP mice

In this study, we mainly investigated the therapeutic effects of rhubarb polysaccharide on the pathological symptoms of HTGAP mice induced by P-407 and L-Arg (Fig. 2A). As shown in **Fig. 2B**, H&E staining of pancreatic tissue revealed an intact pancreatic structure in the control group, while the model group exhibited diffuse injury characterized by severe interlobular space widening, acinar swelling, and separation, along with significantly elevated histopathological scores ($p < 0.01$). In contrast, mice treated with RP maintained a relatively intact pancreatic architecture, with mild interlobular space widening and slight acinar swelling. Furthermore, serum levels of amylase (AMY) and lipase (LPS) were significantly reduced in the RP-treated group compared to the model group (Fig. 2C-D).

H&E staining of intestinal tissue demonstrated normal colonic morphology in the control group, including an intact villus structure, absence of inflammatory cell infiltration, and no submucosal edema. The model group displayed severe pathological alterations, such as prominent inflammatory cell infiltration in the submucosa, moderate necrosis of mid-villus regions, and epithelial cell damage, accompanied by markedly increased histopathological scores ($p < 0.01$). Compared to the model group, RP-treated mice showed only mild villous edema,

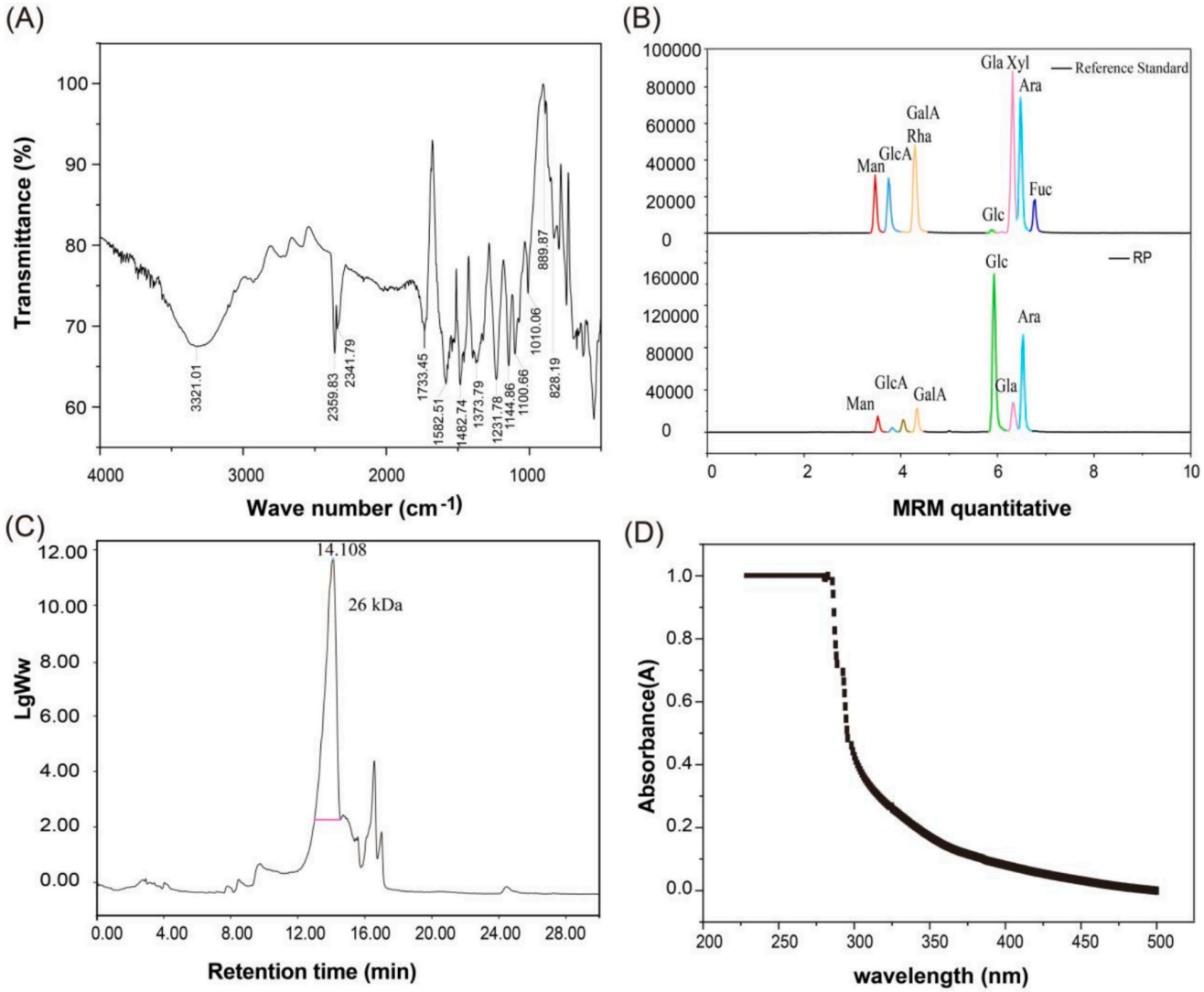

Fig. 1. Structural characterization of RP. (**A**) FT-IR spectrum showing characteristic absorption bands of RP. (**B**) LC-MS extracted ion chromatogram (EIC) of monosaccharide composition derived from hydrolyzed RP. (**C**) Gel permeation chromatography (GPC) profile indicating molecular weight distribution. (**D**) UV–Vis absorption spectrum confirming the absence of nucleic acids or proteins.

repaired epithelial cell layers, and significantly reduced histopathological scores ($p < 0.01$) (Fig. 2E). RT-PCR analysis revealed significant downregulation of ZO-1 and Occludin mRNA levels in the model group, whereas RP treatment effectively reversed these changes (Fig. 2F-G). In addition, two typical markers of the intestinal barrier, ZO-1 and Occludin, were detected by immunohistochemistry. The results showed that the expression levels of ZO-1 and Occludin in the HTGAP group were significantly lower than those in the control group; however, RP treatment increased the expression of ZO-1 and Occludin (Figs. 2H-J). These findings collectively indicate that RP ameliorates intestinal barrier dysfunction in mice with hyperlipidemic acute pancreatitis.

3.3. RP supplementation alleviated gut microbiota dysbiosis in HTGAP mice

To investigate the impact of RP supplementation on gut microbiota composition and function in HTGAP mice, 16S rRNA gene sequencing was performed on intestinal content samples from the NC, HTGAP, and RP groups. We comprehensively assessed the gut microbiota structure using a suite of alpha-diversity indices, including the Chao1 index (richness), Shannon index (diversity), Simpson index (diversity), and Pielou index (evenness). The results indicated that while alpha-diversity remained largely unchanged during HTGAP induction, RP intervention significantly altered microbial diversity (Fig. 3A–D). At the phylum level, HTGAP-induced dysbiosis was characterized by an increase in Firmicutes and Desulfobacterota and a decrease in Proteobacteria—all of which were reversed by RP treatment. These shifts are visualized in the heatmap (Fig. 3E) and further quantified in bar charts depicting relative abundances (Fig. 3F–H). A total of 495 bacterial species were identified at a 97 % similarity threshold, and their mean relative abundances across the three groups are displayed on a phylogenetic tree constructed from representative 16S rRNA gene sequences of each species. The results showed that the abundances of 37 bacterial species differed significantly between the NC and HTGAP groups, among which 16 species exhibited significant improvement after RP treatment. Additionally, RP treatment led to significant changes in the abundances of 45 bacterial species compared to the NC group (Fig. 3I). PCA based on weighted UniFrac distances was used to evaluate β-diversity across groups. Although the NC and HTGAP groups were not completely separated, their distribution exhibited a discernible divergence. In

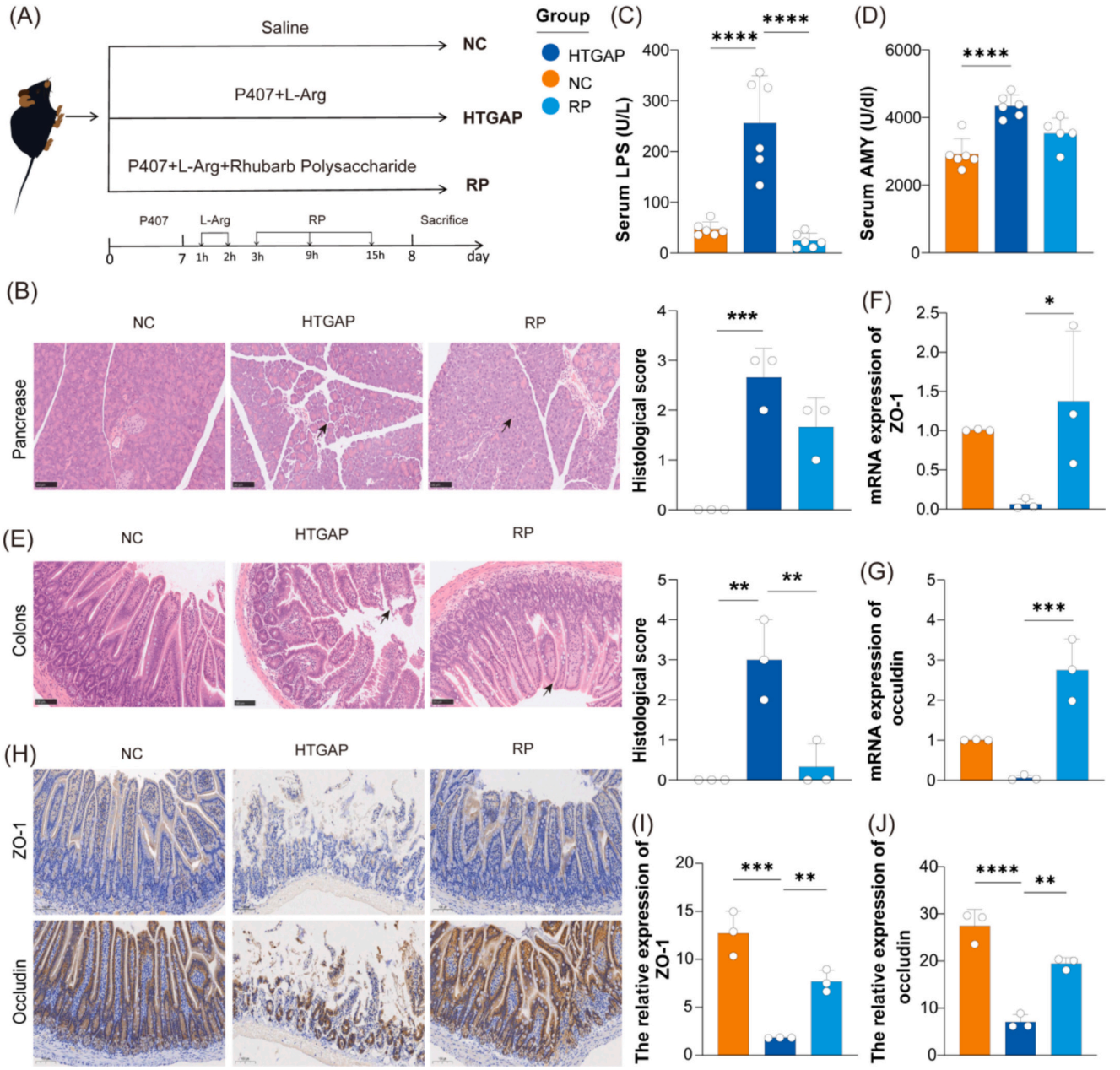

Fig. 2. Rhubarb polysaccharide supplementation alleviated pathological symptoms of HTGAP. (**A**) Schematic diagram of HTGAP model induction via P407 and L-arginine injections, followed by intervention with RP. (**B**) Representative H&E staining images showing morphological characteristics of the mouse pancreas ($n = 3$, magnification: ×400; scale bar: 50 μm), with statistical analysis of histological scores. (**C**) Serum levels of LPS. (**D**) Serum levels of AMY. (**E**) Representative H&E staining images showing morphological characteristics of the mouse colon (n = 3, magnification: ×400; scale bar: 50 μm), with statistical analysis of histological scores. (**F**) Quantitative RT-PCR analysis of ZO-1 expression in the mouse colon (n = 3). (**G**) Quantitative RT-PCR analysis of occludin expression in the mouse colon (n = 3). (**H**) Representative immunohistochemical images of ZO-1 and occludin in colonic tissue. (**I-J**) Quantitative analysis of ZO-1 and Occludin expressions in immunohistochemical staining (n = 3). Data are presented as mean ± SEM (n = 3–6). Statistical analysis was performed using one-way ANOVA followed by Tukey's post hoc test: * $p < 0.05$, ** $p < 0.01$, *** $p < 0.001$.

contrast, the RP group clustered distinctly from the HTGAP group, indicating that RP intervention significantly restructured the gut microbiota in HTGAP mice (Fig. 3J). The PCA loading plot (Fig. 3K) further illustrates the key genera—represented by species arrows—that drove this separation, confirming that shifts in these taxa primarily contributed to the observed differences in microbial community structure. Among the bacterial species, eight showed significant abundance variations. Compared to the NC group, HTGAP mice displayed increased intestinal abundances of *Lachnoclostridium*, *Alistipes indistinctus*, *Desulfovibrio*, *Oscillospiraceae*, *Tuzzerella*, *Bilophila*, GCA-900066575 and *Muribaculum*, which were reduced by RP supplementation (Figs. 3L–3S). To further elucidate the modulatory effects of RP on beneficial gut microbiota in HTGAP mice, we analyzed the relative abundance of several key beneficial bacterial species (Fig. 3T–3W). The results demonstrated that the relative abundances of *Lactobacillus*, *Akkermansia muciniphila*, *Bacteroides acidifaciens*, and *Parasutterella* were significantly reduced in the HTGAP group compared with the NC group. Notably, RP intervention effectively restored the populations of all four beneficial

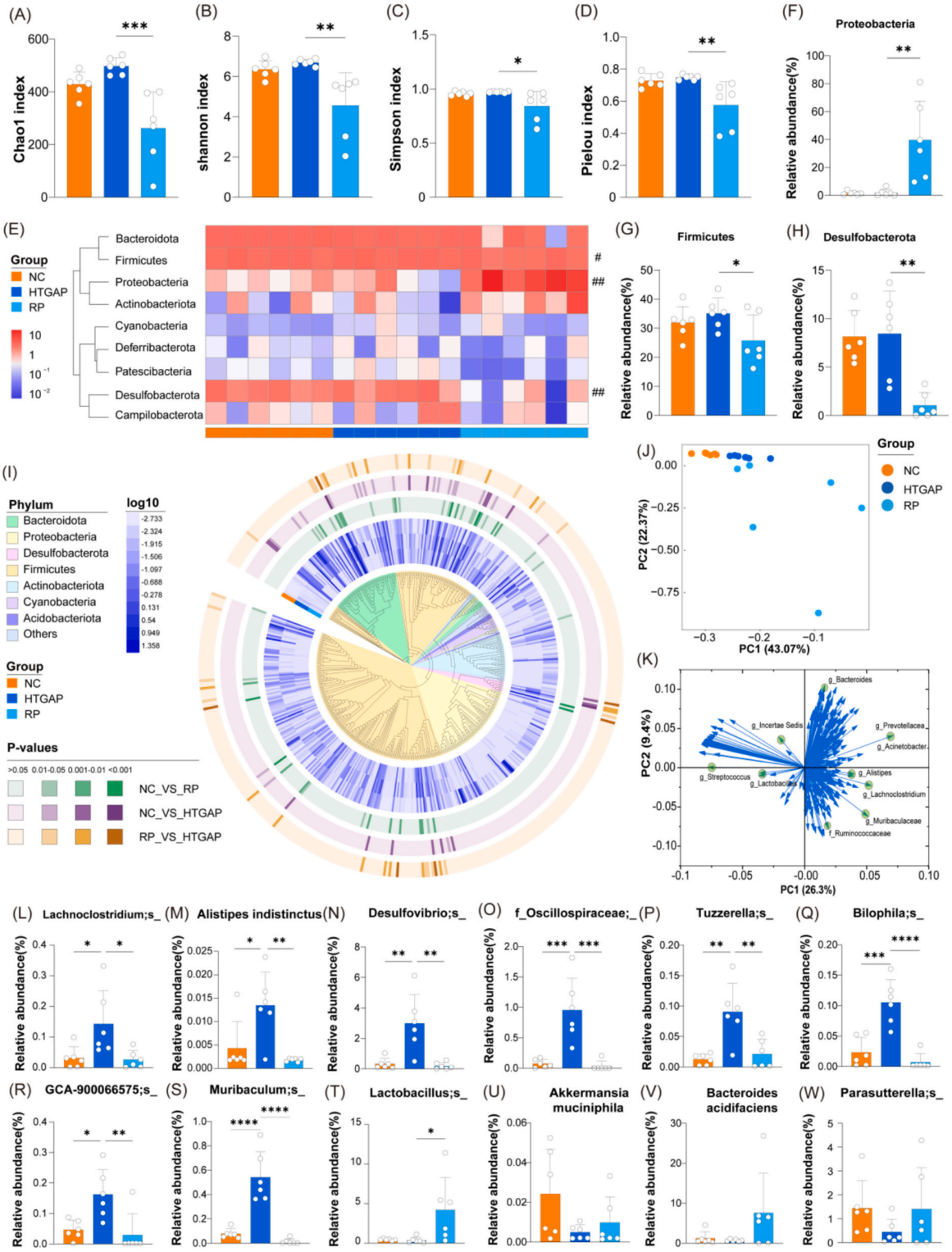

Fig. 3. Rhubarb polysaccharide supplementation alleviates gut microbiota dysbiosis in HTGAP mice. (**A**) Chao1 index. (**B**) Shannon index. (**C**) Simpson index. (**D**) Pielou index. (**E**) Relative abundance of gut microbiota at the phylum level. Relative abundance of phylum level: (**F**) *Proteobacteria,* (**G**) *Firmicutes,* (**H**) *Desulfobacterota.* (**I**) Relative abundance at the species level. (**J**) PCA of species-level microbiota. (**K**) PCA loading plot. Relative abundance of significantly altered bacterial taxa: (**L**) *Lachnoclostridium* bacterium, (**M**) *Alistipes indistinctus* bacterium, (**N**) *Desulfovibrio* bacterium, (**O**) *Oscillospiraceae* bacterium, (**P**) *Tuzzerella* bacterium, (**Q**) *Bilophila* bacterium, (**R**) *GCA-900066575* bacterium, (**S**) *Muribaculum* bacterium, (**T**) *Lactobacillus* bacterium, (**U**) *Akkermansia muciniphila* bacterium, (**V**) *Bacteroides acidifaciens* bacterium, (**W**) *Parasutterella* bacterium. Data are presented as mean ± SEM ($n = 6$). Statistical significance: * $p < 0.05$, ** $p < 0.01$, *** $p < 0.001$ vs. control group; $^{\#}$ $p < 0.05$, $^{\#\#}$ $p < 0.01$, $^{\#\#\#}$ $p < 0.001$ vs. HTGAP group (one-way ANOVA with Tukey's post hoc test).

bacteria. These findings indicate that RP supplementation modulates gut microbiota composition by specifically enhancing the abundance of beneficial microbes such as *Lactobacillus* and *Akkermansia muciniphila*, which may contribute to the restoration of intestinal homeostasis in HTGAP mice.

3.4. RP supplementation altered intestinal metabolites in HTGAP mice

Subsequently, high-resolution LC-MS was used to analyze the metabolite composition in the cecal contents of the three groups of mice under both positive and negative ion modes. A total of 6763 metabolites were detected, of which 3522 could be classified into 28 metabolite categories according to the Kyoto Encyclopedia of Genes and Genomes (KEGG) compound classification system. These categories mainly included antibiotics, peptides, steroids, nucleic acids, hormones and neurotransmitters, vitamins and cofactors, carbohydrates, lipids, and organic acids. The distribution of these different metabolite categories is shown in Fig. 4A. KEGG pathway enrichment analysis further revealed that the differentially abundant metabolites were predominantly associated with tryptophan metabolism, phenylpropanoid biosynthesis, and biosynthesis of plant secondary metabolites, among which tryptophan metabolism exhibited the most significant *p*-value (Fig. 4B). As shown in the Venn diagram (Fig. 4C), the three groups shared 6129 overlapping metabolites, indicating that these substances are common across all groups. Additionally, the NC group contained 103 unique metabolites, the HTGAP group had 84, and the RP group exhibited 213 unique metabolites.

To maximize the visualization of separation between the predefined experimental groups, a supervised multivariate analysis, partial least squares-discriminant analysis (PLS-DA), was performed. The PLS-DA score plots in positive and negative ion modes demonstrated distinct clustering of metabolic compositions across groups following different treatment regimens (Figs. 4D-E), with samples from the same group clustering closely. In positive ion mode, the first two components accounted for 22.6 % and 22.8 % of the variation, respectively, while in negative ion mode, they explained 30.1 % and 19.3 %. The RP group was positioned closer to the NC group, whereas the HTGAP group was markedly separated from the NC group. These results indicate that RP supplementation induced substantial modifications to the metabolic composition of intestinal contents in HTGAP mice.

Subsequent in-depth analysis focused on metabolites with significant differences among the three experimental groups. The volcano plot

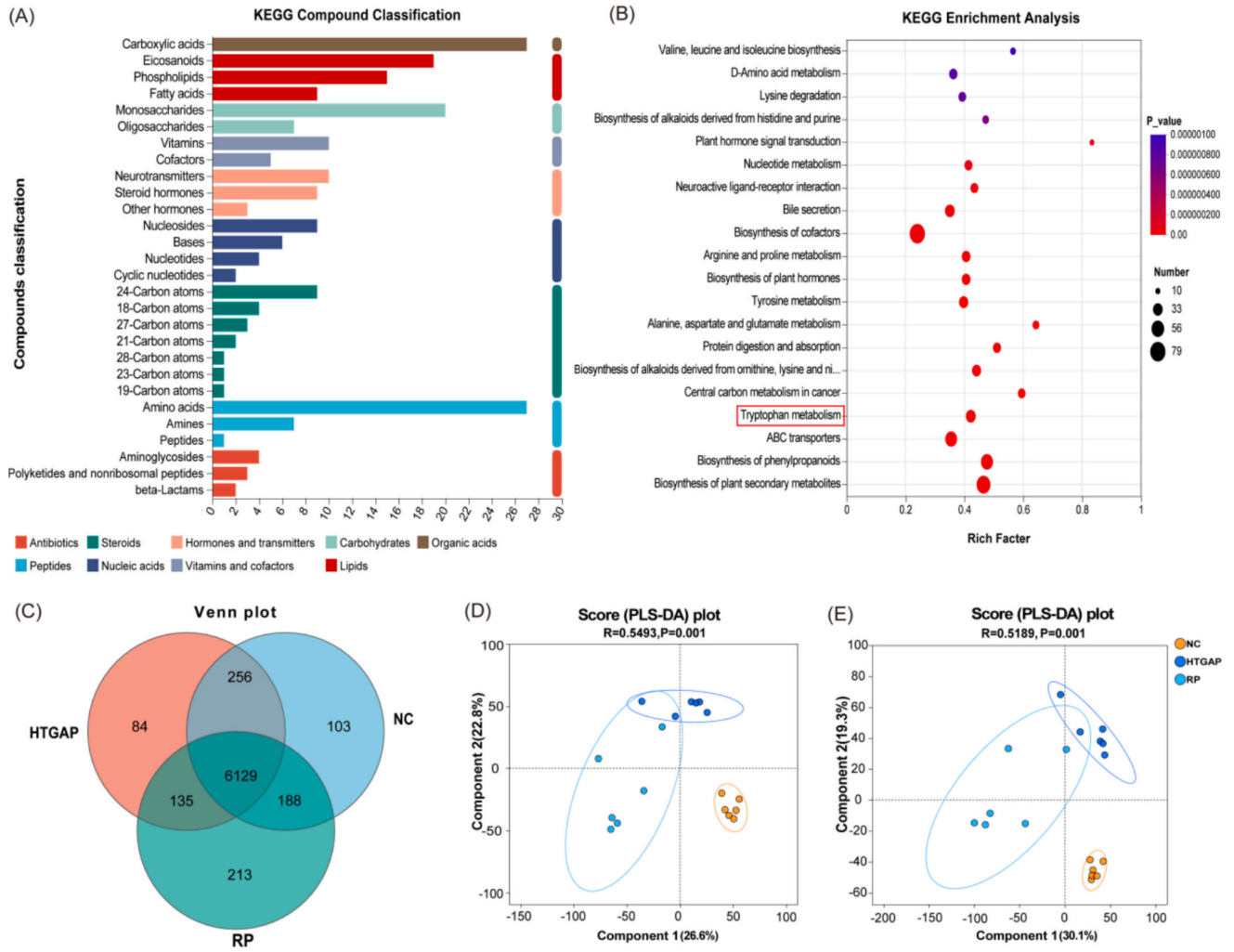

Fig. 4. Rhubarb polysaccharide supplementation alters gut metabolites in HTGAP mice. (**A**) Kyoto Encyclopedia of Genes and Genomes(KEGG)compound classification of metabolites in the three mouse groups. (**B**) Bubble plot displays the KEGG pathway enrichment analysis of differential gut metabolites between NC group mice HTGAP group mice and RP group mice (n = 6/group). The bubble size represents the number of enriched metabolites, and the bubble color indicates the level of enrichment significance (*p*-value). (**C**) Venn diagram of metabolites across the three mouse groups. (**D**) PLS-DA score plot of metabolic profiles in intestinal content samples under positive ion mode. (**E**) PLS-DA score plot of metabolic profiles in intestinal content samples under negative ion mode.

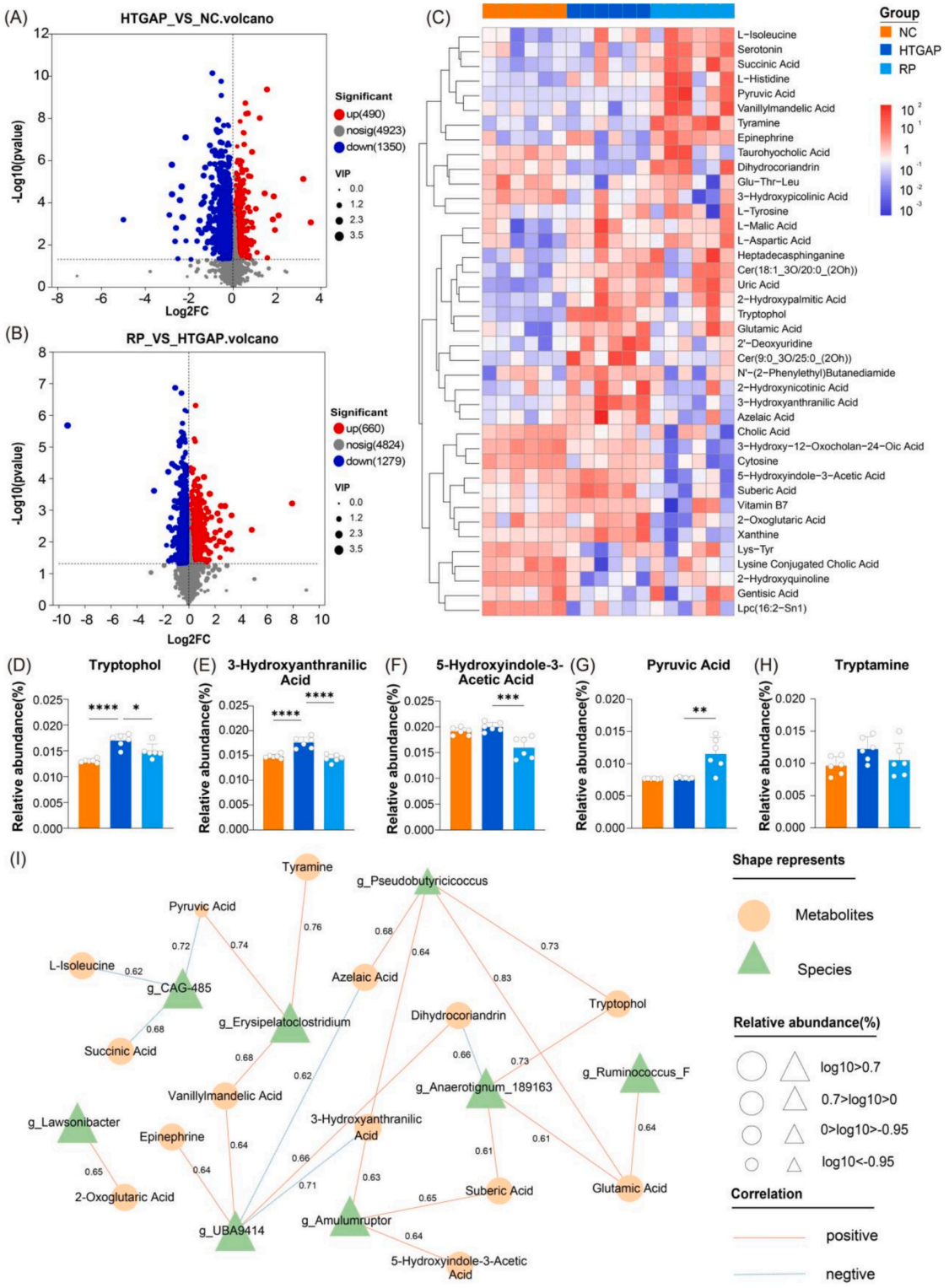

Fig. 5. Rhubarb polysaccharide supplementation alters gut microbial metabolites in HTGAP mice. (**A**) Volcano plot comparing the AP group and the control group. (**B**) Volcano plot comparing the HTGAP group and the AP group. (**C**) Heatmap of clustered overlapping metabolites. (**D**) Tryptophol, (**E**) 3-Hydroxyanthranilic Acid, (**F**) 5-Hydroxyindole-3-Acetic Acid, (**G**) Pyruvic Acid, (**H**) Tryptamine. (**I**) Interaction network between differential metabolites and microbes. The node fill color represents the classification of microbes and metabolites, the node size reflects the relative abundance proportion of each species across different classifications, and the edges between nodes indicate a correlation coefficient greater than 0.6. Data are presented as mean ± SEM (n = 6). Statistical analysis was performed using one-way ANOVA followed by Tukey's post hoc test: * $p < 0.05$, ** $p < 0.01$, *** $p < 0.001$.

(Fig. 5A) revealed that 490 metabolites were significantly upregulated, while 1350 were downregulated in the THGAP group compared to NC, demonstrating a substantial impact of HTGAP on the fecal metabolome. RP treatment further modulated metabolite levels in HTGAP mice (Fig. 5B). Fig. 5C presents a heatmap illustrating the distribution patterns of all annotated metabolites exhibiting intergroup variations, while the remaining figures display bar charts depicting the specific relative abundances of key molecules within each group. The tryptophan metabolite tryptophol, produced by intestinal microbiota, exhibited a pronounced rise in HTGAP model mice, which was substantially reversed upon RP intervention (Fig. 5D), highlighting its potential role in indirectly modulating gut microbiota homeostasis by alleviating intestinal inflammatory responses. The increased levels of the tryptophan metabolite 3-hydroxyanthranilic acid (3-HAA) in the HTGAP group may be associated with excessive inflammatory responses, potentially contributing to the pathogenesis of pancreatitis through gut microbiota-host interactions (Fig. 5E). The tryptophan-derived metabolites 5-hydroxyindole-3-acetic acid (5-HIAA), pyruvic acid, and tryptamine demonstrated differential changes in HTGAP mice upon RP intervention, suggesting broader impacts on tryptophan metabolism (Fig. 5F-H). To analyze the interactions between microbiota and metabolites, Spearman correlations were assessed between all differentially abundant microbiota and metabolites, and a network diagram of microbiome and metabolome features was plotted (Fig. 5I). The figure reveals that g_*Anaerotignum*_189163 exhibits a positive correlation with tryptophol ($r = 0.73$), which may be produced via tryptophan decarboxylation and could be associated with gut-neural regulation. In contrast, g_CAG-485 shows negative correlations with succinic acid ($r = 0.68$), pyruvic acid ($r = 0.72$), and L-Isoleucine ($r = 0.62$), suggesting that this microbial group may regulate amino acid metabolism by influencing the tricarboxylic acid (TCA) cycle, a central metabolic hub where the carbon skeletons of certain amino acids are oxidized for energy or utilized for gluconeogenesis. These findings imply that the coordinated reversal of multiple tryptophan metabolites by RP—as one of the most significantly altered pathways—suggests a potential role of this pathway in its therapeutic mechanism, possibly acting in concert with other important pathways such as biosynthesis of plant secondary metabolites.

4. Discussion

Polysaccharides from *Rheum tanguticum* (*R. tanguticum* polysaccharide) have been isolated and characterized by various research groups. Zhang et al. reported that the polysaccharides they obtained exhibited an average molecular weight of approximately 1840 kDa and were mainly composed of arabinose, galactose, galacturonic acid, and glucose (Zhang et al., 2022). In contrast, Wu et al. isolated *R. tanguticum* polysaccharide with an average molecular weight of about 257 kDa, with galacturonic acid, arabinose, and galactose as the predominant monosaccharide components (Wu et al., 2022). In the present study, the extracted polysaccharides displayed a molecular weight of 26 kDa and were primarily composed of glucose, arabinose, galacturonic acid, and galactose. These results suggest that while the molecular weight of *R. tanguticum* polysaccharide can vary considerably depending on the source or extraction method, their monosaccharide composition remains relatively consistent. However, notable differences exist in the specific proportions of these monosaccharides. Collectively, these findings highlight the structural diversity of *R. tanguticum* polysaccharide and emphasize the importance of further research into their quality control and structure–activity relationships.

R. tanguticum polysaccharide has demonstrated a range of pharmacological activities, particularly in the context of gastrointestinal and metabolic disorders. Previous studies have shown that it can effectively alleviate dextran sulfate sodium (DSS)-induced ulcerative colitis in mice, likely through its ability to modulate the gut microbiota (Zhang et al., 2023). In addition, it has been reported to restore intestinal barrier integrity in mice with NAFLD by upregulating tight junction proteins and reducing inflammatory responses (Qiu et al., 2025). In the present study, *R. tanguticum* polysaccharide significantly alleviated HTGAP-induced elevations in serum amylase and lipase levels. Furthermore, it exhibited protective effects on both pancreatic and intestinal tissues, partially through the regulation of tight junction proteins such as ZO-1 and Occludin. These findings collectively suggest that rheum polysaccharide exerts multifaceted protective effects, likely through anti-inflammatory actions, gut microbiota modulation, and enhancement of barrier function, thereby highlighting its potential as a therapeutic agent for metabolic and intestinal disorders.

Our study provides evidence that RP modulates the gut microbial community structure in HTGAP mice. An invitro fermentation study has shown that indigestible RP can modulate gut microbiota homeostasis by selectively promoting the growth of beneficial bacteria (Kong et al., 2021; Wu et al., 2021; Zhang et al., 2020), particularly probiotics such as *Bacteroides*, *Lactobacillus*, and *Bifidobacterium*. In colitis models (Zhang et al., 2023), *R. tanguticum* polysaccharide intervention effectively alleviated colonic tissue damage while increasing the relative abundance of *Alloprevotella* and reducing harmful bacterial populations such as *Lachnospiraceae_NK4A136_group*, *Allobaculum*, *Parasutterella*, and *Ruminococcus*. In the present study, we found that *R. tanguticum* polysaccharide supplementation significantly reduced the elevated abundances of *Lachnoclostridium*, *Alistipes indistinctus*, *Desulfovibrio*, *Oscillospiraceae*, *Tuzzerella*, *Bilophila*, and *Muribaculum* observed in HTGAP mice. These bacteria are often associated with diet–induced dysbiosis and inflammatory responses. Notably, *Muribaculum* plays a key role in maintaining intestinal homeostasis, metabolic regulation, and immune balance. Previous studies have reported an inverse correlation between *Muribaculaceae* abundance and inflammation severity in colitis models (Yamane et al., 2021; Yan et al., 2019). Concurrently, RP intervention promoted the restoration of beneficial bacteria, including *Lactobacillus*, *Akkermansia muciniphila*, and *Bacteroides acidifaciens*, which are known to contribute to gut barrier integrity and immune regulation. *Akkermansia muciniphila* is widely recognized as a promising next-generation probiotic, whose abundance is closely associated with improved metabolic health, enhanced intestinal barrier function, and reduced systemic inflammation (Xie et al., 2025). Together, these findings suggest that *R. tanguticum* polysaccharide may exert intestinal protective effects in HTGAP by reshaping gut microbiota composition simultaneously suppressing pro-inflammatory bacterial populations and enhancing beneficial taxa thereby contributing to the restoration of microbiota-driven immune and metabolic homeostasis.

Integrated analysis of microbiota and metabolome data revealed that the therapeutic effect of RP is associated with the regulation of microbial metabolic pathways, particularly tryptophan metabolism. Previous studies have demonstrated that in HTGAP mice, hypertriglyceridemia-induced alterations in gut microbiota can upregulate glycerophospholipid metabolism and elevate lysophosphatidylcholine (LysoPC) levels through a TLR4-dependent mechanism, thereby aggravating pancreatic injury during acute pancreatitis (Song et al., 2025). In addition, reduced abundance of *Bacteroides uniformis* in HTGAP has been linked to impaired taurine synthesis, further contributing to metabolic dysregulation and inflammation (Li et al., 2023). RP have been reported to restore disrupted bile acid and free fatty acid metabolism in alcoholic fatty liver disease, thereby exerting hepatoprotective effects against NAFLD (Qiu et al., 2025). In the present study, KEGG enrichment analysis of shared differential metabolites identified tryptophan metabolism as one of the most significantly perturbed pathways, a finding consistent with prior reports (Wang et al., 2025). We further demonstrated that RP intervention effectively reversed HTGAP-induced alterations in key tryptophan metabolites—tryptophol, 3-HAA, 5-HIAA and tryptamine. Given the established role of tryptophan metabolism in modulating host immunity, gut barrier function, and microbe–host crosstalk, our results highlight the gut microbiota–metabolite axis as a critical mediator of HTGAP progression. These insights position the microbial regulation of tryptophan metabolism as a promising target for

therapeutic intervention.

Despite these meaningful findings, several limitations of this study should be acknowledged. The results demonstrate correlations rather than causal relationships. Although the microbiota–tryptophan metabolism axis may be involved in the mechanism by which RP alleviate HTGAP, functional validation experiments—such as fecal microbiota transplantation, antibiotic depletion models, or interventions using specific pathway agonists or antagonists—are still lacking. Furthermore, the potential influence of trace non-polysaccharide components (e.g., anthraquinones) cannot be completely excluded. The specificity of RP as the sole active component requires further confirmation using higher-purity samples and comparative studies with other constituents.

5. Conclusions

In conclusion, this study demonstrates that RP, with a defined molecular weight of 26 kDa and composed primarily of glucose and arabinose, effectively alleviates HTGAP in mice. Treatment with RP markedly attenuated pancreatic tissue injury and restored intestinal barrier function, as evidenced by the upregulated expression of the tight junction proteins ZO-1 and Occludin. Moreover, RP intervention notably remodeled the gut microbiota by suppressing potentially harmful genera (e.g., *Lachnoclostridium*, *Desulfovibrio*) while enriching beneficial bacteria such as *Lactobacillus*, *Akkermansia muciniphila*. Integrated multi-omics analysis further revealed that the therapeutic benefits of RP are closely linked to the regulation of gut microbiota-dependent tryptophan metabolism, highlighted by the reversal of specific metabolite disturbances. Collectively, these findings provide mechanistic insights into how RP alleviates HTGAP and underscore its potential as a therapeutic agent targeting the gut-microbiota-metabolite axis.

6. Perspective

While this study offers substantial insights, several questions remain open for future investigation. First, the causal relationships among RP intervention, microbial shifts, and host metabolic responses need to be definitively established via fecal microbiota transplantation and antibiotic depletion models. Second, the mechanistic specificity of RP—particularly its role in regulating key tryptophan metabolic pathways—warrants further elucidation using highly purified polysaccharide fractions and pathway-specific inhibitors or agonists. Comparative studies with other rhubarb-derived components would also help clarify the unique contribution of polysaccharides. Addressing these questions will deepen the mechanistic understanding of RP's therapeutic actions and facilitate its development as a targeted strategy for HTGAP and related metabolic disorders.

CRediT authorship contribution statement

Ya Chen: Writing – original draft, Investigation, Data curation, Conceptualization. **Wen-Wen Zhang:** Investigation, Data curation, Conceptualization. **Yun-Yun Mao:** Investigation, Data curation. **Gang-Ao Hu:** Investigation, Data curation. **Xin-Xin Chen:** Investigation, Data curation. **Yi-Lin Zhou:** Formal analysis, Data curation. **Xiao-Long Chen:** Formal analysis, Data curation. **Hong Wang:** Writing – review & editing, Project administration, Funding acquisition. **Bin Wei:** Writing – review & editing, Project administration, Funding acquisition. **Jian-Feng Tu:** Writing – review & editing, Project administration, Funding acquisition.

Ethics statement

All animal experiments were conducted in accordance with the Guide for the Care and Use of Laboratory Animals and were approved by the Animal Ethics Committee of Zhejiang University of Technology (Approval No.: ZH20240716021).

Funding statement

This work was supported by the "Pioneer" and "Leading Goose" R&D Program of Zhejiang Province (No.2025C02180), the international (regional) cooperation and exchange program jointly initiated by the National Natural Science Foundation of China (No. W2412100), and the National Key Research and Development Program (No. 2022YFC2804700).

Declaration of competing interest

The authors declare that they have no known competing financial interests or personal relationships that could appear to influence the work reported in this paper.

Data availability

Data will be made available on request.

References

Cao, Y.-J., Pu, Z.-J., Tang, Y.-P., Shen, J., Chen, Y.-Y., Kang, A., Zhou, G.-S., & Duan, J.-A. (2017). Advances in bio-active constituents, pharmacology and clinical applications of rhubarb. *Chinese Medicine, 12*, 36. https://doi.org/10.1186/s13020-017-0158-5

Wu, Ding-Tao, Yuan, Qin, Feng, Kang-Lin, Zhang, Jinming, Gan, Ren-You, Zou, Liang, Wang, & Shengpeng. Fecal fermentation characteristics of Rheum tanguticum polysaccharide and its effect on the modulation of gut microbial composition *Chinese Medicine, 17*(1), (2022). https://doi.org/10.1186/s13020-022-00631-6

Du, X., B., M., .l., Shichiyakh, R., Haque, M. A., Aubakirov, M., Syamsu, J. A., & Khan, A. (2025). Eubiotics improve gut health and overall production in animals by reducing pathogenic bacteria. *Pakistan Veterinary Journal, 45*(2), 488–498, 10.29261/pakvetj/2025.186.

Gou, H., Su, H., Liu, D., Wong, C. C., Shang, H., Fang, Y., … Yu, J. (2023). Traditional medicine Pien Tze Huang suppresses colorectal tumorigenesis through restoring gut microbiota and metabolites. *Gastroenterology, 165*(6), 1404–1419. https://doi.org/10.1053/j.gastro.2023.08.052

Gubensek, J. (2023). The role of apheresis and insulin therapy in hypertriglyceridemic acute pancreatitis—A concise review. *BMC Gastroenterology, 23*, 341. https://doi.org/10.1186/s12876-023-02957-3

Hu, X., Gong, L., Zhou, R., Han, Z., Ji, L., Zhang, Y., … Wu, D. (2021). Variations in gut microbiome are associated with prognosis of hypertriglyceridemia-associated acute pancreatitis. *Biomolecules, 11*(5), 695. https://doi.org/10.3390/biom11050695

Iqbal, T., Altaf, S., Fatima, M., Rasheed, R., Laraib, K., Azam, M., … Usman, S. (2024). A narrative review on effective use of medicinal plants for the treatment of parasitic foodborne diseases. *Agrobiological Records, 16*, 79–92. https://doi.org/10.47278/journal.abr/2024.016

Kong, Q., Zhang, R., You, L., Ma, Y., Liao, L., & Pedisić, S. (2021). In vitro fermentation characteristics of polysaccharide from Sargassum fusiforme and its modulation effects on gut microbiota. *Food and Chemical Toxicology, 151*, Article 112145. https://doi.org/10.1016/j.fct.2021.112145

Li, G., Liu, L., Lu, T., Sui, Y., Zhang, C., Wang, Y., Zhang, T., Xie, Y., Xiao, P., Zhao, Z., Cheng, C., Hu, J., Chen, H., Xue, D., Chen, H., Wang, G., Kong, R., Tan, H., Bai, X., & Sun, B. (2023). Gut microbiota aggravates neutrophil extracellular traps-induced pancreatic injury in hypertriglyceridemic pancreatitis. *Nature Communications, 14*(1). https://doi.org/10.1038/s41467-023-41950-y

Liu, J., Yan, Q., Li, S., Jiao, J., Hao, Y., Zhang, G., … Shang, D. (2024). Integrative metagenomic and metabolomic analyses reveal the potential of gut microbiota to exacerbate acute pancreatitis. *npj Biofilms and Microbiomes, 10*(1), 29. https://doi.org/10.1038/s41522-024-00499-4

Lyu, F., Han, F., Ge, C., Mao, W., Chen, L., Hu, H., Chen, G., Lang, Q., & Fang, C. (2023). OmicStudio: A composable bioinformatics cloud platform with real-time feedback that can generate high-quality graphs for publication. *Imeta, 2*(1), Article e85. https://doi.org/10.1002/imt2.85

Pan, Y., Li, Y., Gao, L., Tong, Z., Ye, B., Liu, S., Li, B., Chen, Y., Yang, Q., Meng, L., Wang, Y., Liu, G., Lu, G., Li, W., & Li, J. (2017). Development of a novel model of hypertriglyceridemic acute pancreatitis in mice. *Scientific Reports, 7*, Article 40799. https://doi.org/10.1038/srep40799

de Pretis, N., Amodio, A., & Frulloni, L. (2018). Hypertriglyceridemic pancreatitis: Epidemiology, pathophysiology and clinical management. *United European Gastroenterology Journal, 6*(5), 649–655. https://doi.org/10.1177/2050640618755002

Qiu, J., Xu, F., Wei, H., Gao, Y., Liu, N., Zhao, J., Yu, Z., Chen, L., & Dou, X. (2025). Metabolic restoration: Rhubarb polysaccharides as a shield against non-alcoholic fatty liver disease. *International Journal of Biological Macromolecules, 305*, Article 141151. https://doi.org/10.1016/j.ijbiomac.2025.141151

Shen, X.-H., Guan, J., Lu, D.-P., Hong, S.-C., Yu, L., & Chen, X. (2024). Peptostreptococcus Anaerobius enhances dextran sulfate sodium-induced colitis by promoting nf-κB-NLRP3-dependent macrophage pyroptosis. *Virulence, 15*(1), Article 2435391. https://doi.org/10.1080/21505594.2024.2435391

Song, K., Wu, Z., Meng, J., Tian, W., Zheng, S., Mu, D., Wang, R., Pang, H., & Wu, D. (2023). Hypertriglyceridemia as a risk factor for complications of acute pancreatitis and the development of a severity prediction model. *HPB: The Official Journal of the International Hepato Pancreato Biliary Association, 25*(9), 1065–1073. https://doi.org/10.1016/j.hpb.2023.05.006

Song, X., Qiao, L., Dou, X., Chang, J., Zeng, X., Deng, T., Yang, G., Liu, P., Wang, C., Xu, Q., & Xu, C. (2025). Hypertriglyceridemia-modulated gut microbiota promotes lysophosphatidylcholine generation to aggravate acute pancreatitis in a TLR4-dependent manner. *iMeta, 4*(1), Article e70003. https://doi.org/10.1002/imt2.70003

Syed-Abdul, M. M., Tian, L., Hegele, R. A., & Lewis, G. F. (2025). Futility of plasmapheresis, insulin in normoglycaemic individuals, or heparin in the treatment of hypertriglyceridaemia-induced acute pancreatitis. *The Lancet. Diabetes & Endocrinology, S2213-8587*(25). https://doi.org/10.1016/S2213-8587(25)00028-2, 00028–2.

Wang, D., Sun, S., Zhao, Q., Zhao, B., Ma, L., Su, T., Xu, L., Gui, M., Xu, D., Chen, W., Zeng, Y., Shen, Y., Liu, Y., Jiang, C., Ni, Q., Cui, Y., Lu, Y., Lu, Q., Dong, D., & Mao, E. (2025). Metabolic shifts in tryptophan pathways during acute pancreatitis infections. *JCI Insight, 10*(5), Article e186745. https://doi.org/10.1172/jci.insight.186745

Wen, Y., Han, C., Liu, T., Wang, R., Cai, W., Yang, J., … Xia, Q. (2020). Chaiqin chengqi decoction alleviates severity of acute pancreatitis via inhibition of TLR4 and NLRP3 inflammasome: Identification of bioactive ingredients via pharmacological sub-network analysis and experimental validation. *Phytomedicine: International Journal of Phytotherapy and Phytopharmacology, 79*, Article 153328. https://doi.org/10.1016/j.phymed.2020.153328

Wu, C., Yang, F., Zhong, H., Hong, J., Lin, H., Zong, M., Ren, H., Zhao, S., Chen, Y., Shi, Z., Wang, X., Shen, J., Wang, Q., Ni, M., Chen, B., Cai, Z., Zhang, M., Cao, Z., Wu, K., & Liu, R. (2024). Obesity-enriched gut microbe degrades myo-inositol and promotes lipid absorption. *Cell Host & Microbe, 32*(8), 1301–1314.e9. https://doi.org/10.1016/j.chom.2024.06.012

Wu, D.-T., Yuan, Q., Guo, H., Fu, Y., Li, F., Wang, S.-P., & Gan, R.-Y. (2021). Dynamic changes of structural characteristics of snow chrysanthemum polysaccharides during in vitro digestion and fecal fermentation and related impacts on gut microbiota. *Food Research International, 141*, Article 109888. https://doi.org/10.1016/j.foodres.2020.109888

Wu, H., Tremaroli, V., Schmidt, C., Lundqvist, A., Olsson, L. M., Krämer, M., … Bäckhed, F. (2020). The gut microbiota in prediabetes and diabetes: A population-based cross-sectional study. *Cell Metabolism, 32*(3), 379–390.e3. https://doi.org/10.1016/j.cmet.2020.06.011

Xie, J., Du, L., Lu, Y., Guo, X., Zhou, X., Tong, Y., Shen, B., Yu, X., Guo, F., & Yu, H. (2025). Akkermansia muciniphila alleviates severe acute pancreatitis via Amuc1409-Ube2k-Foxp3 axis in regulatory T cells. *Advanced Science, 12*(30), Article e04214. https://doi.org/10.1002/advs.202504214

Xu, X., Xu, H., Shang, Y., Zhu, R., Hong, X., Song, Z., & Yang, Z. (2021). Development of the general chapters of the chinese pharmacopoeia 2020 edition: A review. *Journal of Pharmaceutical Analysis, 11*(4), 398–404. https://doi.org/10.1016/j.jpha.2021.05.001

Yamane, T., Handa, S., Imai, M., Harada, N., Sakamoto, T., Ishida, T., Nakagaki, T., & Nakano, Y. (2021). Exopolysaccharides from a Scandinavian fermented milk viili increase butyric acid and Muribaculum members in the mouse gut. *Food Chemistry: Molecular Sciences, 3*, Article 100042. https://doi.org/10.1016/j.fochms.2021.100042

Yan, S., Yang, B., Zhao, J., Zhao, J., Stanton, C., Ross, R. P., … Chen, W. (2019). A ropy exopolysaccharide producing strain *Bifidobacterium longum* subsp. *Longum* YS108R alleviates DSS-induced colitis by maintenance of the mucosal barrier and gut microbiota modulation. *Food & Function, 10*(3), 1595–1608. https://doi.org/10.1039/C9FO00014C

Yang, J., Han, F., Wu, G., Dong, Y., Su, H., Xu, J., & Li, J. (2023). Dysregulated B7H4/JAK2/STAT3 pathway involves in hypertriglyceridemia acute pancreatitis and is attenuated by baicalin. *Digestive Diseases and Sciences, 68*(2), 478–486. https://doi.org/10.1007/s10620-022-07606-5

Yang, J., Tang, X., Wu, Q., Ren, P., & Yan, Y. (2022). A severe acute pancreatitis mouse model transited from mild symptoms induced by a "two-hit" strategy with L-arginine. *Life, 12*(1), 126. https://doi.org/10.3390/life12010126

Yang, Q., Luo, Y., Ge, P., Lan, B., Liu, J., Wen, H., … Chen, H. (2023). Emodin ameliorates severe acute pancreatitis-associated acute lung injury in rats by modulating exosome-specific miRNA expression profiles. *International Journal of Nanomedicine, 18*, 6743–6761. https://doi.org/10.2147/IJN.S428924

Yao, W., Xie, Z., Li, M., Zhang, M., Dai, W., Duan, B., Wang, M., Tang, C., & Yang, Z. (2024). Hypertriglyceridemic acute pancreatitis: A bibliometric analysis from 2002 to 2023. *International Journal of Surgery (London, England), 111*(1), 1484–1487. https://doi.org/10.1097/JS9.0000000000001935

Yi, X., Lu, W., Liu, D., Zhuang, H., Peng, C., Ge, Y., … Ma, C. (2025). Psyllium and inulin supplementation alleviates diarrhea and supports gut flora in pre-weaning calves. *Pakistan Veterinary Journal, 45*(3), 1061–1072.

Yu, Y., Wang, H., Jin, X., Huang, W., Zhao, Y., Wang, N., … Wang, H. (2025). Structural characterization of Dendrobium officinale polysaccharides and their regulation effect on intestinal microbiota during in vitro fermentation. *Polymers, 17*(6), 727. https://doi.org/10.3390/polym17060727

Zhang, D., Liu, J., Cheng, H., Wang, H., Tan, Y., Feng, W., & Peng, C. (2022). Interactions between polysaccharides and gut microbiota: A metabolomic and microbial review. *Food Research International, 160*, Article 111653. https://doi.org/10.1016/j.foodres.2022.111653

Zhang, X., Liu, Y., Chen, X.-Q., Aweya, J. J., & Cheong, K.-L. (2020). Catabolism of Saccharina japonica polysaccharides and oligosaccharides by human fecal microbiota. *LWT, 130*, Article 109635. https://doi.org/10.1016/j.lwt.2020.109635

Zhang, Y., Liu, Y., Luo, J., Liu, Y., Yu, S., & Jia, L. (2023). Rheum tanguticum polysaccharide alleviates DSS-induced ulcerative colitis and regulates intestinal microbiota in mice. *Food Bioscience, 53*, Article 102788. https://doi.org/10.1016/j.fbio.2023.102788